Thermal analysis of a double excitation synchronous machine

Trung-Kien Hoang, Vido Lionel, F Gillon, M. Gabsi

THERMAL ANALYSIS OF A DOUBLE EXCITATION SYNCHRONOUS MACHINE

K. Hoang[1], L. Vido[2], F. Gillon[3], and M. Gabsi[1]

[1] SATIE, ENS Cachan, 94235 Cachan, France
e-mail : kienht26@gmail.com
[2] SATIE, University of Cergy-Pontoise, 33 bd du Port, 95000 Cergy-Pontoise, France
[3] L2EP, Ecole Centrale de Lille, 59650 Villeneuve d'Ascq Cedex, France

Abstract - In this paper, a thermal analysis of a synchronous machine using the double excitation principle is presented. Two global field windings introduce not only a more complicated structure but also additional heat sources and heat evacuation difficulties. In this research, the thermal analysis is accomplished by using a lumped parameter model, and results are compared with experiments.

Keyword - Double excitation, thermal network, permanent magnet.

1 INTRODUCTION

A Double Excitation Synchronous Motor (DESM) has been proved to be efficient as it combines advantages of a wound field synchronous motor, which is the field weakening control, and a permanent magnet synchronous motor with high efficiency and high power density [1–6]. The presence of field windings actually not only creates additional heat sources but also alters some heat evacuation paths inside the machine. For certain types of DESM with very complicated mechanical structures, an accurate thermal analysis is hard to handle. There has been a big number of researches dedicated to electromagnetic designs of different types of DESM [1–7]. To the knowledge of author, however, efforts to examine the thermal aspect of this kind of machine seems to be quite few, [3] as an example. Thermal researches for this kind of machine are, therefore, necessary.

This paper is dedicated to the thermal analysis of a parallel type of DESM. The lumped parameter thermal network (LPTN), which is a very common method for a thermal analysis, is used. Thermal resistance calculations is a big challenge as they often require empirical formulations, and those values usually have significant impacts on the result. In this paper, thermal coefficients are determined by experiments. This paper is constructed as follows: section 2 introduces the DESM prototype. Then, the LPTN is addressed in section 3 with heat source and some main thermal resistances calculations. Section 4 is dedicated to the determination of thermal coefficients by experiments. Results are shown in section 5 followed by a conclusion.

2 DESM PROTOTYPE

A number of motor prototypes using double principle has been realized according to different criteria. Concerning the localization of the excitation flux sources, both sources can be placed in the stator and/or rotor. Regarding how flux sources are combine, a DESM can be classified as series or parallel ones. Fig. 1 shows the DESM prototype used in this paper [1].

This topology belongs to the parallel type, which was proved to be advantageous over the series counterpart in respect of controlling the open circuit flux [8]. The main reason to choose the parallel type is due to the fact that the main flux path generated by field windings does not pass through permanent magnets (PMs). In this prototype, two global field windings are placed on the stator side, this arrangement helps to avoid sliding contacts. Ferrite PMs locates in the rotor using flux concentration principle to increase air-gap flux. Details of the prototype are given in Table. 1.

In this prototype, some motor flux lines are truly three dimensional (3-D) as in [1], so that solid core materials are advised to employ in some regions as marked in Fig. 1(a). As seen in Fig. 1(b), tow field windings are attached to the outer-stator core and placed right above the armature end-winding regions. This arrangement will alter the heat evacuation part of the armature end-winding since more heat will be evacuated through these field windings.

3 LUMPED THERMAL ANALYSIS NETWORK

3.1 GENERAL THERMAL MODEL

The thermal analysis model based on lumped parameters is to benefit from fast calculations while maintain-

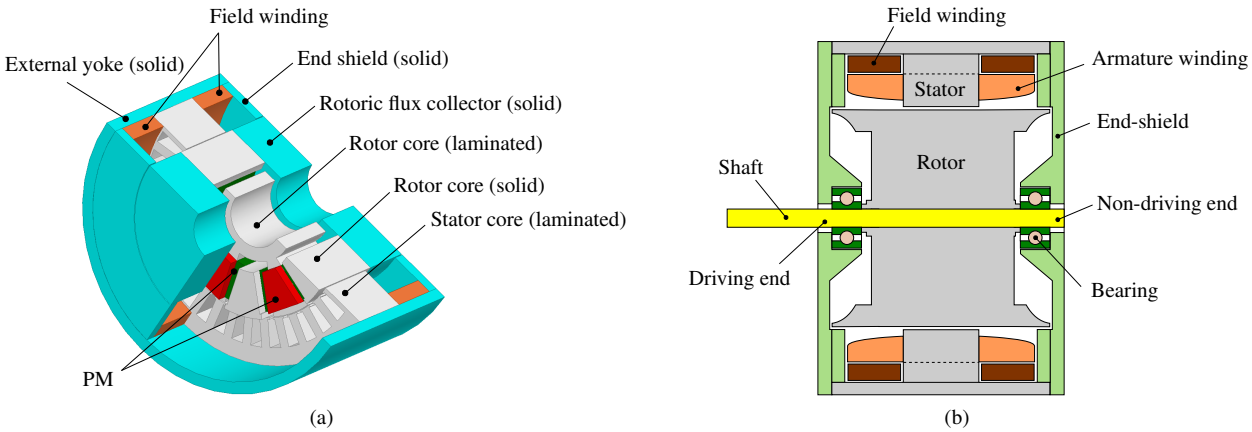

Fig. 1. DESM prototype. (a) Prototype. (b) Overall mechanical structure

I. Reference DESM model configuration

Parameters	Value
Number of phases	3
Number of turns per phase	33
Number of turns per field winding	150
Number of poles	12
Motor length	115 mm
Outer stator diameter	92 mm
Inner stator diameter	57.5 mm
Number of slots	36
Air-gap length	0.5 mm
PM residual flux density	0.4 T (ferrite PM)
Based speed	2000 rpm
Rated power	3 kW
Cooling type	Natural air

ing a good accuracy for overall temperatures. The thermal network is presented in Fig. 2, which is capable of considering the transient process by introducing thermal heat capacitors.

As it can be seen in Fig. 2, two types of thermal resistance are presented: one uses a simple coefficient, and the other needs empirical coefficients. The first one is computed based on the geometry of the object, while the second is more difficult and coefficients based on experiments or design experiences are desirable. It should be noted that the prototype is naturally cooled by ambient air. This means that the surface thermal resistance is pretty high with a low heat transfer coefficient. Some important points about the thermal analysis in this paper are listed as below:

1. Heat sources mainly consist of core and copper losses. Mechanical losses will be proved small.

2. Three heat transfer phenomena are considered:

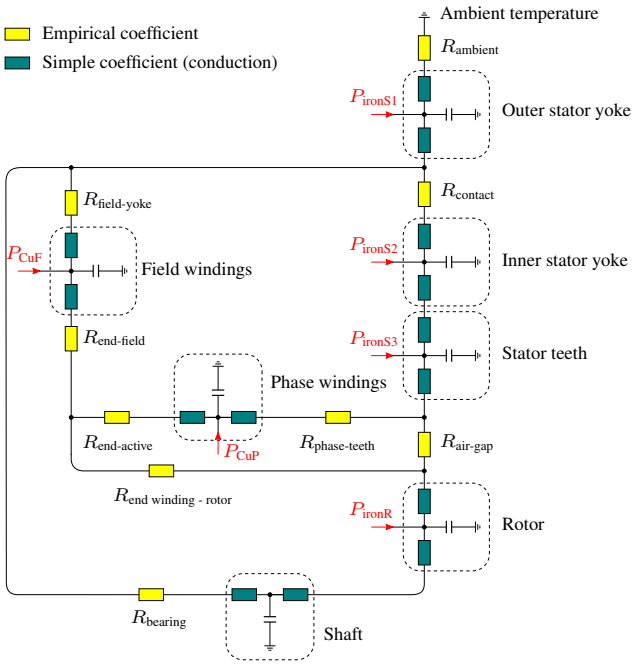

Fig. 2. Thermal network. Thermal resistances: $R_{\text{field-yoke}}$ - between field winding and outer stator yoke, $R_{\text{end-field}}$ - between armature end and field windings, $R_{\text{end-active}}$ - between armature end and active parts, $R_{\text{end-rotor}}$ - between armature end winding and rotor surface, $R_{\text{phase-teeth}}$ - between armature active winding and stator teeth, $R_{\text{air-gap}}$ - air gap, R_{bearing} - bearing. Losses: P_{CuF} - field winding copper losses, P_{CuP} - armature copper loss, P_{ironS1} - outer stator yoke core loss, P_{ironS2} - inner stator yoke core loss, P_{ironS3} - stator teeth core loss, P_{ironR} - rotor core loss

- Convection on the surface and air environment inside machine.
- Radiation on the surface.
- Conduction in copper windings and core.

3. The transient mode is solved by assuming losses are constant in a short period of time. Copper

losses are updated after each period when winding temperatures are obtained.

3.2 HEAT SOURCE CALCULATIONS

Heat sources includes core loss, copper loss, mechanical and windage losses. The unit core loss [W/m^3] is calculated as (1) [9]. This formula considers harmonic contents.

$$P_{\text{Fe}} = k_h f \hat{B}^{\alpha} + \frac{k_e}{2\pi^2 T} \int_0^T \left(\frac{dB}{dt} \right)^2 dt \qquad (1)$$

where k_h, α and k_e are core loss coefficients determined from sample measurements, f is frequency of flux density waveform, and $T = 1/f$.

The copper loss is computed by (2)

$$P_{\text{Cu}} = I^2 R \left[1 + \beta(\theta - 20)\right] \qquad (2)$$

where I is RMS current, R is winding resistance at 20°C , β is thermal coefficient of winding at 20°C , and θ is winding temperature.

The mechanical loss consists of windage and bearing friction losses, which are calculated as (3a) [10] and (3b), respectively.

$$P_{\text{windage}} = \pi C_d \rho R^4 \omega^3 L_a \qquad (3a)$$

$$P_{\text{bearing}} = 5.013 \cdot 10^{-4} \mu_f P_{eb} \omega d \qquad (3b)$$

where ρ is air density [kg/m^3], R is average air-gap diameter [m], ω is rotor angular speed [rad/s], L_a is axial length [m], C_d is skin friction coefficient. μ_f is friction coefficient, P_{eb} is equivalent dynamic bearing load [N], and d is bearing diameter [mm].

3.3 SURFACE THERMAL RESISTANCE CALCULATION

Since the machine uses natural air cooling, the heat evacuation through the stator surface to the ambient becomes difficult. This is due to the very low heat transfer coefficient. Two heat transfer processes are included namely convection and radiation.

The convection process depends on the surface area and surface temperature θ_s, surface orientation i.e horizontal or vertical, and ambient-air temperature θ_a. The typical outer frame of a horizontal electrical machine is shown in Fig. 3

Following assumptions are made:

- Uniform temperature θ_s on the outer-stator surface.
- Two vertical plates are identical.

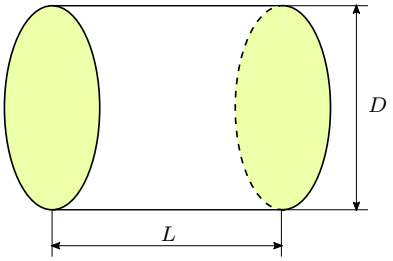

Fig. 3. Outer frame configuration

- Average surface emissivity are used.

The equivalent convective resistance is derived as (4). This calculation is resulted from the parallel connection between convective resistances due to the horizontal cylinder surface S_1 and two vertical plates S_2.

$$R_c = \frac{1}{h_1 S_1 + 2h_2 S_2} = \frac{1}{h_c S} \qquad (4)$$

where h_c is equivalent convective coefficient, and S is total surface.

From (4), h_c can be computed as (5):

$$\begin{aligned} h_c &= \frac{h_1 S_1 + 2h_2 S_2}{S_1 + 2S_2} \\ &= \frac{h_1 \pi \frac{D^2}{4} + h_2 \pi D L}{\pi \frac{D^2}{4} + \pi D L} \\ &= \frac{h_1 D + 2h_2 L}{D + 2L} \end{aligned} \qquad (5)$$

The radiative heat transfer facilitates the heat evacuation from the machine especially in natural air convection circumstances. The radiative heat transfer strongly depends not only on the surface and ambient temperatures but also on the surface property, which is characterized by the emissivity coefficient ϵ. This coefficient is not practically constant, instead, it varies with the temperature, color, and surface material [11]. That makes the analysis quite complex. In this paper, the emissivity is assumed constant across the outer-stator surface.

The thermal resistance due to radiative heat transfer is given by (6):

$$R_r = \frac{1}{h_r S} \qquad (6)$$

where h_r is radiative heat transfer coefficient expressed by (7) [11].

$$h_r = \frac{\epsilon \sigma_c \left(\theta_s^4 - \theta_a^4\right)}{\theta_s - \theta_a} = \epsilon \sigma_c \left(T_s + T_a\right) \left(\theta_s^2 + \theta_a^2\right) \qquad (7)$$

where σ_c is Stefan-Boltzmann constant ($5.67 \cdot 10^{-8}$ W/m^2/K^4), and θ_s and θ_a are surface and ambient temperatures, respectively.

The equivalent surface heat transfer coefficient is derived by summing up the individual ones h_c and h_r as (8)

$$h_e = \frac{1}{R_s S} = h_c + h_r \tag{8}$$

3.4 THERMAL RESISTANCE BETWEEN ARMATURE ACTIVE WINDING AND STATOR CORE

The thermal resistance between the copper core of the armature winding and the stator core is of importance because this big resistance is on the main path of evacuating the armature copper loss to the ambient. Fig. 4 demonstrates an armature winding in the slot with several material layers.

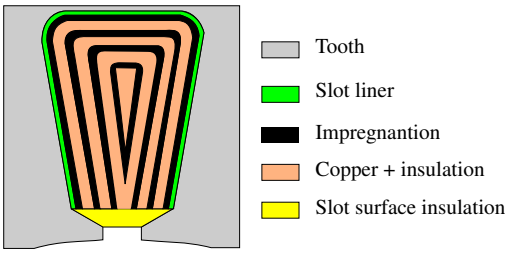

Fig. 4. Winding insulation in the slot

Staton *et al.* [12] proposed an equivalent thermal conductivity between the copper part and iron core $k_{\text{cu,ir}}$. This equivalent conductivity depends on a couple of factors such as the material, quality of the impregnation, and filling factor. The approximation is experimentally proposed as (9) as a function of the filling factor k_f. The It is noted that the filling factors for those tests varied between 0.35 and 0.45. That value of the DESM prototype in this paper is 0.35.

$$k_{\text{Cu,ir}} = 0.1076 \cdot k_f + 0.029967 \tag{9}$$

It should be noted that in case of no copper presented ($k_f = 0$), $k_{\text{cu,ir}}$ is 0.029967 which is the thermal conductivity of the air (at 80°C).

The thermal resistance between the copper and iron core is determined as (10).

$$R_{\text{Cu,ir}} = \frac{S_{\text{slot}}(1 - k_f)}{k_{\text{Cu,ir}} l_{\text{sp}}^2 L_s} \tag{10}$$

where l_{sp} is stator slot perimeter, L_s is active stack length, and S_{slot} is stator-slot surface.

3.5 THERMAL RESISTANCE BETWEEN FIELD WINDINGS AND STATOR CORE

The double excitation principle presents additional field windings, this makes the machine complicated not only about the electromagnetic analysis but also the thermal one. The main reason is the "non-standard" assembly of these field windings. Unlike the armature windings, where the manufacturing and assembly processes would be standardized, and formulations for its thermal resistance is, therefore, widely available. No similar researches for that of the global field windings in the studied DESM. A field winding is shown in Fig. 5. As it can be seen, the contact surface between the winding and core is smaller than that of a winding located in the slot. Moreover, this contact is not so tight i.e. a big air space is presented between the windings and stator core. These explain why heat evacuation for the field windings of the prototype is difficult.

II. Static measurements

Case	I_a [A]	I_f [A]
1	4	0
2	0	4
3	4	4

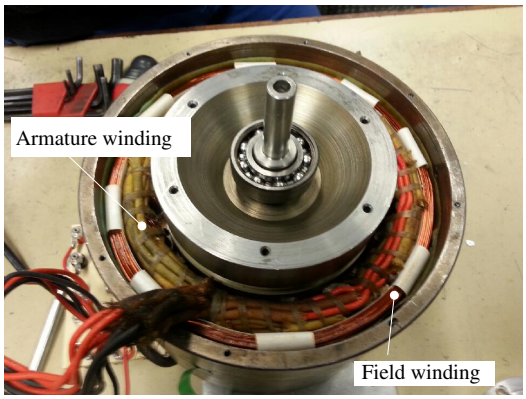

Fig. 5. Field winding of the studied DESM

The residual air and contact surface between the field windings and motor core (especially to the end-shield side) is difficult to determine. A correction factor α_f will be applied to formula (10). Experiments are later on performed to determine this correction factor.

4 THERMAL COEFFICIENTS CALIBRATION BY EXPERIMENTS

In this part, several thermal coefficients will be experimentally calibrated. In detail, static experiments are carried out meaning that no core losses due to rotations. Copper losses of the field and armature windinngs will be measured. Experimental setup is displayed in Fig. 6.

There are three static thermal measurements are carried out with details are as shown in Table. 2. In these tests, three armature windings are connected in series, and so do the two field windings. In test 3, all five winding are connected in series. In all tests, windings are supplied with DC currents.

Surface heat transfer coefficients are shown in Fig. 7.

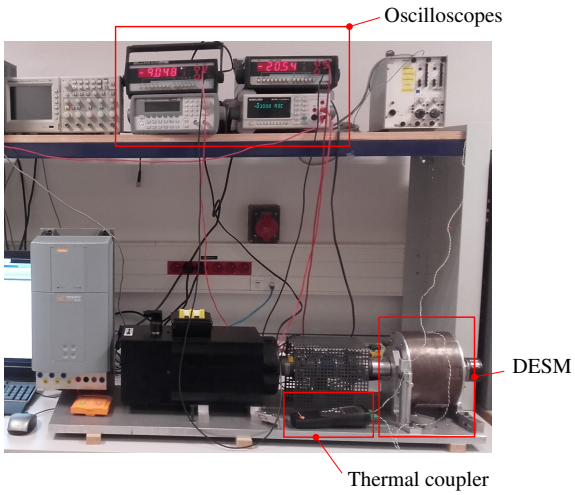

Fig. 6. Thermal experimental setup

As it will be seen, there are differences between measured and calculated values. This can be explained by the fact that actual surface emissivities across the outer surface are not constant. More importantly, the machine in the experiment is coupled with some components, which certainly increases equivalent surface for heat evacuation. Therefore, a correction factor of 1.2, i.e. 20% increase, is applied to this coefficient.

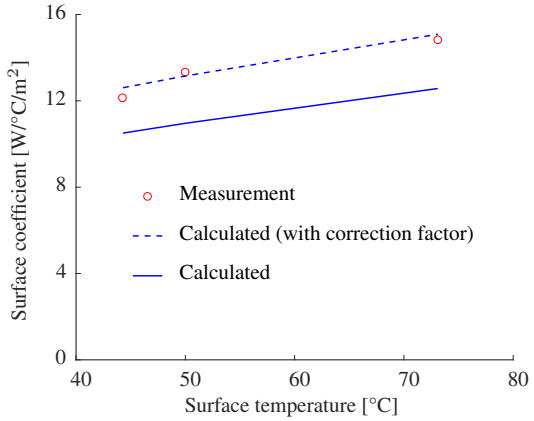

Fig. 7. Surface coefficient according to surface temperature at 20 °C ambient temperature

The coefficient α_f for the field windings is determined as 2.5, meaning that a big adjustment (2.5 times) applied to (10). This is due to very big thermal resistances between the field windings and stator core.

5 Result and Experimental Validation

Comparisons between the analysis and experiments in the transient mode are shown in Fig. 8. As it will be seen, a good accordance is reported. Due to the natural air convection on the surface, the overall temperatures are pretty high even though the heat sources, i.e. copper losses, are low. In case 3, for instance, the total copper loss is only about 75 W.

6 Conclusion

The thermal analysis of a double excitation synchronous machine has been discussed. The machine's particularity in both theoretical and practical (due to assembly process) aspects makes it challenging for an accurate thermal analysis. Due to the empirical thermal equations used, experimental calibrations for some coefficients are necessary. The final analysis in a transient mode was compared to experiments with a quite acceptable accordance. The analysis could help to propose some cooling conditions to improve machine performances, such as improvement in the thermal contact between the field windings and the iron core to extend the thermal limit of the field windings, the utilization of field windings is, therefore, improved.

References

[1] L. Vido, M. Gabsi, M. Lecrivain, Y. Amara, and F. Chabot, "Homopolar and bipolar hybrid excitation synchronous machines," in *Electric Machines and Drives, 2005 IEEE International Conference on*, May 2005, pp. 1212–1218.

[2] E. Hoang, M. Lecrivain, and M. Gabsi, "A new structure of a switching flux synchronous polyphased machine with hybrid excitation," in *European Conference on Power Electronics and Applications*, Sept. 2007, pp. pp.1–8.

[3] D. Fodorean, A. Djerdir, I. A. Viorel, and A. Miraoui, "A double excited synchronous machine for direct drive application: Design and prototype tests," *Energy Conversion, IEEE Transactions on*, vol. 22, no. 3, pp. 656–665, Sept 2007.

[4] Y. Amara, L. Vido, M. Gabsi, E. Hoang, A. Hamid Ben Ahmed, and M. Lecrivain, "Hybrid excitation synchronous machines: Energy-efficient solution for vehicles propulsion," *Vehicular Technology, IEEE Transactions on*, vol. 58, no. 5, pp. 2137–2149, Jun 2009.

[5] R. Owen, Z. Zhu, and G. Jewell, "Hybrid-excited flux-switching permanent-magnet machines with iron flux bridges," *Magnetics, IEEE Transactions on*, vol. 46, no. 6, pp. 1726–1729, June 2010.

[6] B. Nedjar, S. Hlioui, Y. Amara, L. Vido, M. Gabsi, and M. Lecrivain, "A new parallel double excitation synchronous machine," *Magnetics, IEEE Transactions on*, vol. 47, no. 9, pp. 2252–2260, Sept 2011.

[7] K. Hoang, L. Vido, M. Gabsi, and F. Gillon, "Flux control range broadening and torque ripple minimization of a double excitation synchronous motor," *IEEE Transactions on Magnetics*, vol. 53, no. 1, pp. 1–10, Jan 2017.

[8] Y. Amara, S. Hlioui, R. Belfkira, G. Barakat, and M. Gabsi, "Comparison of open circuit flux control capability of a series double excitation machine and a parallel double excitation ma-

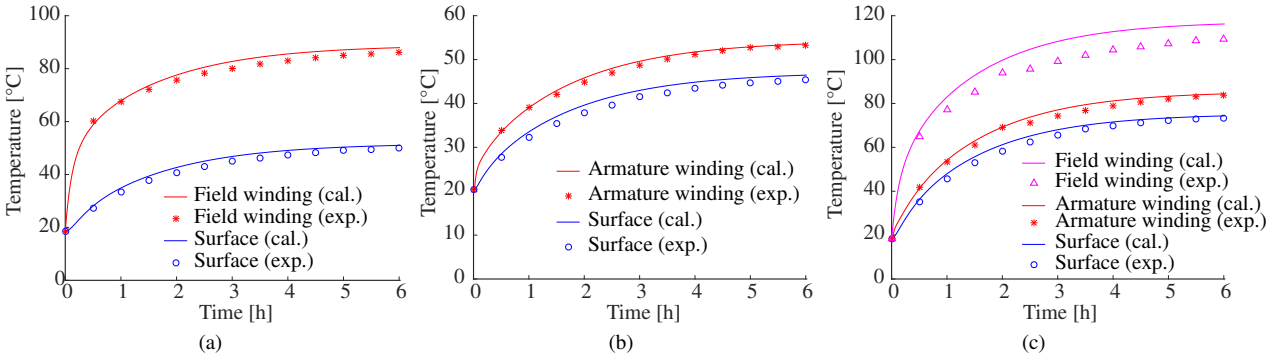

Fig. 8. Comparisons between calculated and experimental temperatures, cal. - calculated, exp. - experiment. (a) Case 1. (b) Case 2. (c) Case 3.

chine," *Vehicular Technology, IEEE Transactions on*, vol. 60, no. 9, pp. 4194–4207, Nov 2011.

[9] D. Lin, P. Zhou, W. Fu, Z. Badics, and Z. Cendes, "A dynamic core loss model for soft ferromagnetic and power ferrite materials in transient finite element analysis," *Magnetics, IEEE Transactions on*, vol. 40, no. 2, pp. 1318–1321, March 2004.

[10] J. E. Vrancik, "Prediction of windage power loss in alternators," NASA, Tech. Rep., October 1968.

[11] Y. Çengel and A. Ghajar, *Heat and Mass Transfer: Fundamentals and Applications*. McGraw-Hill, 2011. [Online]. Available: https://books.google.fr/books?id=P5urQwAACAAJ

[12] D. Staton, A. Boglietti, and A. Cavagnino, "Solving the more difficult aspects of electric motor thermal analysis in small and medium size industrial induction motors," *Energy Conversion, IEEE Transactions on*, vol. 20, no. 3, pp. 620–628, Sept 2005.